EEG Source Imaging Enhances the Decoding of Complex Right-Hand Motor Imagery Tasks

Bradley J. Edelman, Bryan Baxter, and Bin He*, *Fellow, IEEE*

Abstract*—*Goal: **Sensorimotor-based brain–computer interfaces (BCIs) have achieved successful control of real and virtual devices in up to three dimensions; however, the traditional sensor-based paradigm limits the intuitive use of these systems. Many control signals for state-of-the-art BCIs involve imagining the movement of body parts that have little to do with the output command, revealing a cognitive disconnection between the user's intent and the action of the end effector. Therefore, there is a need to develop techniques that can identify with high spatial resolution the self-modulated neural activity reflective of the actions of a helpful output device.** ***Methods:*** **We extend previous EEG source imaging (ESI) work to decoding natural hand/wrist manipulations by applying a novel technique to classifying four complex motor imaginations of the right hand: flexion, extension, supination, and pronation.** ***Results:*** **We report an increase of up to 18.6% for individual task classification and 12.7% for overall classification using the proposed ESI approach over the traditional sensor-based method.** ***Conclusion:*** **ESI is able to enhance BCI performance of decoding complex right-hand motor imagery tasks.** ***Significance:*** **This study may lead to the development of BCI systems with naturalistic and intuitive motor imaginations, thus facilitating broad use of noninvasive BCIs.**

***Index Terms*—Brain–computer interface (BCI), brain mapping, EEG source imaging (ESI), motor imagery (MI), neuroimaging.**

I. Introduction

FOR those people suffering from severe neurological impairments, brain–computer interface (BCI) technology has provided an alternative means of communication with the environment outside of the body's natural neuromuscular pathways [1]. BCIs using intracortically implanted electrode arrays have allowed subjects with severe damage to their descending motor circuitry to successfully control robotic prosthetics with anthropomorphic movement to complete common everyday tasks [2], [3]. These systems are able to exploit the high spatial specificity that can be achieved by targeting individual neurons or neuronal ensembles and the tuning properties of cells in the primary motor cortex (M1). For noninvasive BCIs, the spatial resolution of detectable signals is significantly lower than intracortical recordings, restricting analysis to higher level signals originating from larger populations of synchronized neurons such as the P300 [4]–[6], steady-state visual evoked potentials [7]–[9], slow cortical potentials [10], and sensorimotor rhythms (SMRs) [11], [12]. Of particular promise, SMR-based BCIs have accomplished control of both virtual and real objects in up to three dimensions by identifying unique spatiotemporal dynamics of oscillatory activity originating in the sensorimotor cortex [12]–[18].

Control signals extracted for SMR BCIs are founded on the voluntary modulation of frequency-specific electrical activity in M1. Neurons within the sensorimotor cortex maintain a resting synchrony in the alpha/mu (8–13 Hz) and beta (13–30 Hz) bands that represents an idle motor state. Upon performing motor imagery (MI), in which a motor action is imagined but not executed, local populations of neurons responsible for the imagination desynchronize to process the task and result in a decrease of alpha–beta power. This local desynchronization is accompanied by increased synchronization in the noncontrolling hemisphere or near the midline. These phenomena are termed event-related desynchronization (ERD) and event-related synchronization (ERS), respectively, and occur along the motor homunculus according to the topographic organization of M1 [17]. It is the identification of ERD and ERS among the different recording electrodes overlying M1 that allow the system to recognize which task a user is performing. The BCI then translates the identified MI task into a particular action of the end effector.

Despite the success of SMR BCIs, there are various limitations regarding a user's ability to achieve successful control. Of foremost importance, electroencephalography (EEG) itself suffers from the volume conduction effect, which blurs and distorts neuroelectric signals as they travel from the cortical surface to the scalp [19]. The consequence is a smearing of the ERD and ERS generated in response to MI tasks from adjacent somatotopic regions. The projected scalp patterns from these nearby cortical regions have high spatial correlation and make it exceedingly difficult to distinguish which task is being performed. Therefore, one of the major challenges for high-dimensional BCIs is to overcome the low spatial resolution of EEG by finding optimal combinations of MI tasks and EEG electrodes used to decode the independent activity. In this sense, the most straightforward approach to increasing the dimensionality of SMR BCIs is to utilize the somatotopic organization of M1 by finding MI tasks, which activate regions of the cortex that are distant enough to be separated by the recording electrodes, such as the left and right hand, feet and tongue [20]–[23].

However, this often leads to a cognitive disconnection between the MI task being performed and the corresponding action

Manuscript received February 28, 2015; revised May 12, 2015 and June 27, 2015; accepted July 24, 2015. Date of publication July 24, 2015; date of current version December 17, 2015. This work was supported in part by the National Science Foundation under Grant CBET-1264782 and Grant IGERT DGE-1069104, and in part by the National Institutes of Health under Grant R01 EB006433. *Asterisk indicates corresponding author.*

B. J. Edelman and B. Baxter are with the Department of Biomedical Engineering, University of Minnesota.

*B. He is with the Department of Biomedical Engineering and the Institute for Engineering in Medicine, University of Minnesota, Minneapolis, MN 55455 USA (e-mail: binhe@umn.edu).

Color versions of one or more of the figures in this paper are available online at http://ieeexplore.ieee.org.

Digital Object Identifier 10.1109/TBME.2015.2467312

of the output device. For example, in a representative horizontal 1-D paradigm, left- and right-hand MI is used to drive a computer cursor to the left and right, respectively. These tasks are intuitive and the user's motor intent is effectively reflected by the movement of the cursor. When adding a second dimension, feet and tongue MI tasks are often used to drive the vertical movement of the cursor. These tasks are chosen because they, in addition to right- and left-hand MI, generate spatially distinct patterns in sensor space. However, unlike the horizontal movement, there is no clear mental link between imagining movement of the feet and tongue with the up and down movement of an output device. Therefore, in those high-dimensional paradigms that are able to achieve successful control, the MI tasks used are unnatural and could significantly benefit from new imaginations that better resemble the resulting action of the end effector. Despite these shortcomings, various techniques targeting user training as well as neural signal processing are available to drive SMR BCI toward more realistic control.

Over the past decade, He and colleagues have pursued a source-analysis-based BCI approach [22]–[26]. EEG source imaging (ESI) is used to counteract the volume conduction effect by projecting the scalp potential readings onto a source space representing the geometry of the brain. These techniques reconstruct electrical activity of the gyral and sulcal folds of the brain by modeling populations of cells as equivalent dipoles [24], [25] or current density distributions [22]–[24], [26]. Spatial filters are then generated to determine the relationship between the recording electrodes and dipoles in order to trace electrical activity on the scalp back to specific neuroanatomical structures. ESI has recently received considerable attention in the BCI community because it can identify MI tasks with equal or greater performance than the sensor domain analysis [23], [26]. It is thought that by reconstructing the current density on the cortical surface, *a priori* physiological postulates can inform regions of the brain that are more likely responsible for generating the scalp EEG. In this manner, the source transformed data can be constrained to include information that is more highly correlated with the task being performed, thus reducing extraneous and noisy data [22], [27], [28]. The ability to isolate patches of the cortex on an anatomical basis provides an opportunity to further exploit the somatotopic properties of M1 and extract control signals that are more intuitive for a user to perform.

For BCI applications, detecting downstream actions can vastly increase the dimensionality of the technology and provide the means to customize systems by integrating tasks specific to a user's particular needs. Prosthetic arm control using MI signals has been a long sought after goal for both the rehabilitation of injured brain regions (e.g., stroke patients) and the replacement of limbs that can no longer be controlled (e.g., spinal cord injury, amputation). However, many of the current control signals are unable to provide the user with intuitive and successful control of these devices. For fine motor control of a robotic arm/hand, it would be optimal for the user to perform an MI task involving a particular manipulation of one's own hand and to then have the same action performed by the robot. Despite this great need, few studies have examined the possibility of separating control signals of complex hand MI tasks for SMR BCI use. These analyses have been limited to sensor space data and often have limited classification schemes with modest results.

In summary, the following issues that need to be addressed for SMR BCIs to progress toward everyday use are twofold.

1) The low spatial resolution of EEG significantly limits the number of MI tasks that can be used to successfully control an SMR BCI.
2) MI tasks that generate distinct and usable control signals are not intuitively matched to the action of the output device and make it difficult to provide neurofeedback reflective of the user's intent.

In this paper, we have examined the separability of MI tasks involving four different manipulations of the right hand: flexion, extension, supination, and pronation. These tasks were chosen to represent complex actions involved in fine motor control of the hand which could be applied to both rehabilitative and prosthetic control purposes. With the previous success of ESI for discriminating MI tasks, it is our hypothesis that reconstructing the electrical activity on the cortical surface will allow us to isolate regions containing more discriminable information regarding specific MI tasks of the hand. We greatly improved the discrimination of these tasks by using a source-based approach beyond the peak accuracy achieved by the sensor-based method.

II. Experimental Design and Setup

A. MI Task

Five human subjects (three males, average age of 25.5 $\pm$ 9.7 years) with previous BCI experience participated in this study with written consent to an experimental protocol approved by the University of Minnesota Institutional Review Board. Subjects were seated in a comfortable chair in front of a computer screen and instructed to perform 2-Hz self-paced MI of right-hand flexion, extension, supination, or pronation. Each trial was designed as follows: a "rest" icon initially appeared on the screen for 3 s. This was followed by 3 s of a target indicating which MI task to perform. During this period, the subject was instructed to focus on the computer screen and clear their mind as preparation for the upcoming task. Finally, a 4-s "go" cue was presented during which the subject continuously performed the specified MI task [see Fig. 1(a) and (b)]. A 1-s intertrial interval was appended after the task for additional rest.

For the duration of each run, subjects supported their right arm on the arm rest of the chair and maintained their right hand in a neutral position defined by aligning the wrist to the forearm, with the hand relaxed and thumb oriented upward. Prior to the MI runs, subjects performed motor execution runs of the same tasks as a motor priming stage. During execution, the subject was instructed to focus on the sensation involved in each task which was to be mentally recalled during the imagination.

Flexion and extension (FE) and supination and pronation (SP) MI tasks were paired together and randomized within each run. Each session was composed of four runs of 20 trials for each pair of tasks. The order in which the subjects performed the FE and SP runs alternated for successive sessions. Each subject participated in four sessions on four separate days, with a total of 160 trials allotted to each MI task. The analysis pipeline of

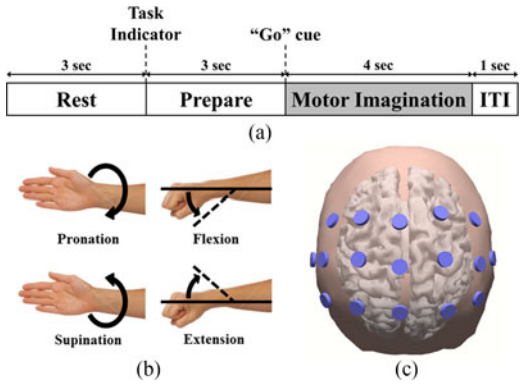

Fig. 1. (a) Trial structure for collecting the MI task data. Flexion and extension, and supination and pronation tasks were paired together within a run. Each run contained 20 trials for each pair of tasks (ten trials per task). (b) Subjects were asked to perform MI of flexion, extension, supination or pronation. (c) Seventeen electrodes overlying the motor cortex were used in this analysis.

the proposed ESI and traditional sensor-based approaches are outlined in Fig. 2 and described in the following sections.

B. EEG Preprocessing

Raw EEG was acquired from 64 channels located according to the standard 10–20 electrode system using a SynAmpsRT amplifier (Neuroscan Compumedics, Singen, Germany) at a sampling frequency of 1 kHz. The 17 electrodes (FC3, FC1, FCz, FC2, FC4, C5, C3, C1, Cz, C2, C4, C6, CP3, CP1, CPz, CP2, CP4) overlying the motor cortex, highlighted in Fig. 1(c), were utilized for this analysis since we were only concerned with motor related activity [24]–[26]. The recorded data were separated into four separate sets, each containing only the trials of one of the MI tasks. EEG recordings were downsampled to 100 Hz and bandpass filtered between 2 and 30 Hz using a zero-phase finite impulse response filter. Trials containing artifactual behavior (i.e., jaw clenching, muscle movement, electrode disconnections, etc.) were removed by visual inspection. A surface Laplacian was then applied to the remaining trials to enhance focal activity related to the MI tasks. Given that the entire trial does not contain information relevant to the MI task, only the data from 1 s prior to the beginning of the task to 1 s after the task ended was kept for further analysis.

C. Cortical Current Density Estimation

In order to convert data from the sensor domain to the source domain, an EEG forward model was first generated to describe the electrical conductance between the scalp sampling sites and the modeled dipolar sources of the brain. Solving the "EEG forward problem" generates a transfer matrix, or lead field, that relates the activity in source space to that of sensor space. This association can be represented by the linear system in (1), where b represents the recorded scalp data, A the lead field, x the source activity, and n the measurement noise:

$$b = Ax + n \tag{1}$$

Solving the "EEG inverse problem" consists of solving (1) for x through the process described in (2), where λ is a regularization parameter and W is a weighting matrix:

$$\min_x ||Ax - b||^2 + \lambda||Wx||^2 \tag{2}$$

In theory, the optimal solution of x would be one that minimizes the residual between the estimated and recorded scalp topographies in the L2 norm least-squares sense, as depicted by the first term in (2). However, because the number of dipoles is often much larger than the number of electrodes, there are many source distributions that can generate similar patterns on the scalp. Tikhonov regularization was therefore employed to further constrain the solution to find the x which minimized the residual as well as the energy of the source solution [29]. This additional constraint is represented by the second term in (2); the influence of the two terms was balanced by the regularization parameter λ, which was found using the L-curve method. For the L2 norm case, the analytic solution to (2) gives rise to the optimal estimate of the source distribution $\hat{x}$, indicated by (3). This transformation, therefore, takes the lead field and scalp potentials as inputs and provides as an output the estimated cortical current density.

$$\hat{x} = A^T \left(AA^T + \lambda W\right)^{-1} b \tag{3}$$

When W is simply the identity matrix, this solution is referred to as the minimum norm estimate (MNE). The MNE, however, is biased by the fact that superficial dipoles will inherently project more strongly to the scalp. This effect was corrected by applying a set of weights to the dipoles such that the influence of dipole depth was reduced; this approach thus becomes the weighted MNE (WMNE) [30].

For this analysis, the Colin27 MRI average brain [31] was used to convert between sensor and source space. The structural MRI volume was initially segmented into five surface layers (white matter, gray matter, cerebral spinal fluid, skull, and scalp). The segmented gray matter was then tessellated into a triangular mesh composed of 8325 equivalent dipoles representing discrete locations on the cortex for which the current density would be solved. The dipoles were fixed with an orientation perpendicular to the gray matter surface to maintain neurophysiological consistency with pyramidal neurons that are responsible for generating the signals detected by EEG. A three-shell conduction model was created to represent the scalp, skull, and inner cerebral tissues using the boundary element method [32], [33], with conductivity values assigned in the ratio of 1:1/15:1 [34]–[36]. Electrode locations were coregistered with the skin using standard anatomical landmarks on the head. The concept of ESI is depicted in Fig. 2.

D. Region of Interest Selection

Where similar ESI studies have selected a region of interest (ROI) by identifying particular gyral landmarks on subject specific cortex models [28], [37], we elected to use a purely data-driven approach to select the right-hand ROI since the same template brain was used for all subjects [38]. In this approach, the preprocessed EEG from all four MI tasks was compiled into a single dataset. This compiled dataset, therefore, contains EEG from all of the MI activity of the right hand.

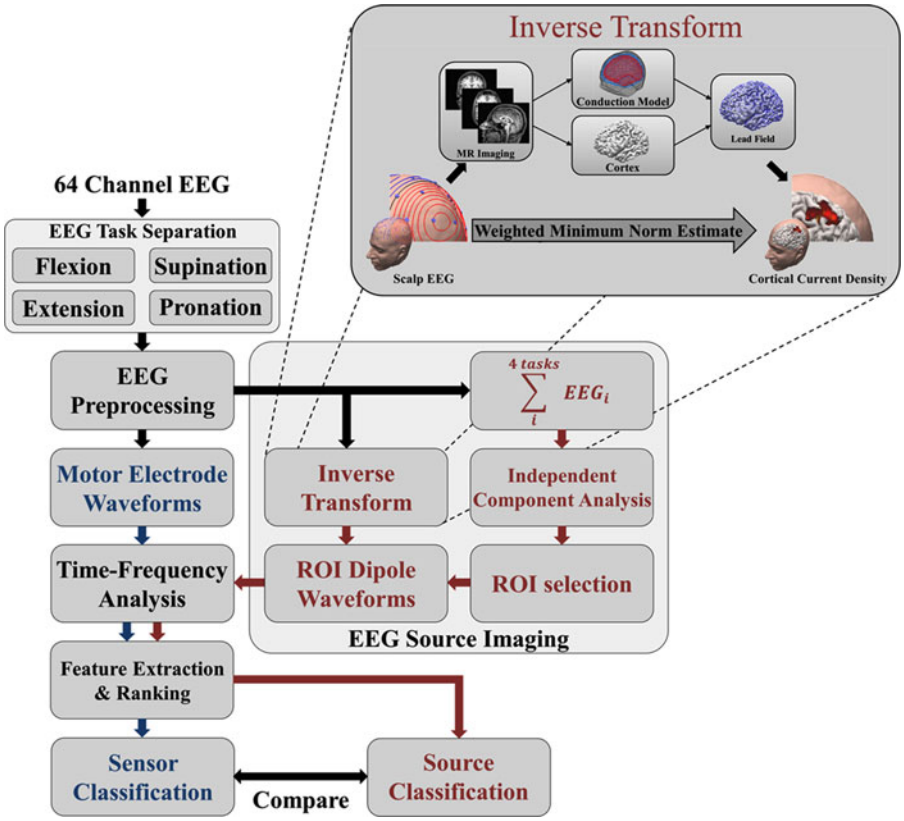

Fig. 2. (Bottom left) Analysis pipeline describing the traditional sensor and proposed source-based approach. Time–frequency features were extracted from the 17 electrode waveforms for classification in the sensor method; time–frequency features were extracted from the waveforms from dipoles within the designated ROI for the source-based method. (Top right) Schematic of ESI; using anatomical MRI data, a three-layer realistic-geometry numerical head model was constructed to solve the EEG inverse problem and project the scalp-recorded EEG onto a cortical surface.

Independent component analysis (ICA) was then used to decompose the compiled dataset into temporally independent sources using the extended InfoMax algorithm [39]. The output of ICA decomposition is composed of an $N_e \times N_e$ weight matrix and an $N_e \times t$ activation matrix, where N_e denotes the number of scalp electrodes and t the number of time points of the original data. Each column of the inverse weight matrix represents the scalp topography associated with a single independent component (IC) and has a corresponding activation sequence within the EEG envelope, indicated by the rows of the activation matrix.

The alpha/mu band ERD has long been shown to be indicative of gross limb activity [17], [40], [41]. Therefore, to determine which of these components contained the motor activity, we constructed a time–frequency representation (TFR) that characterizes the "ideal" event-related activity associated with a motor task, as displayed in Fig. 3(a). Based on the data segments that we chose to include for this analysis, each trial contains three blocks: 1 s of preparation, 4 s of MI, and 1 s of post-task. In the preparation and post-task blocks, we assigned a value of one to the 8–13 Hz frequency band to represent the idling motor activity that would result from not performing MI. During the task block, the 8–13 Hz activity was assigned to zero to signify an ERD associated with performing a motor task. The TFR of each component was found according to the methodology explained in subsequent sections, averaged across trials and normalized to its peak value.

The single component that displayed the highest time–frequency correlation with this ideal MI event-related behavior was selected as that which was thought to be responsible for the overlapping right-hand source activity. Fig. 3(b) illustrates the TFRs from a representative subject for the three components with the highest correlation to the task, along with their respective component topographies. The selected component topography was then mapped onto a template brain using the WMNE and thresholded at 75% of the peak value to identify dipole locations on the cortex to be included in the ROI. The selected IC topographies and ROIs for all subjects are displayed in Fig. 3(c).

E. Feature Extraction and Selection

Features from the individual preprocessed datasets for each of the MI task were extracted independently. For sensor analysis, features were extracted from all electrode time series, and for source analysis, only those dipole time series within the cortical ROI (see Fig. 2). TFRs of the selected waveforms were obtained using a Morlet wavelet approach. The wavelet was initially designed at a central frequency f_c where its temporal resolution, or manifested length, is defined by the full-width at

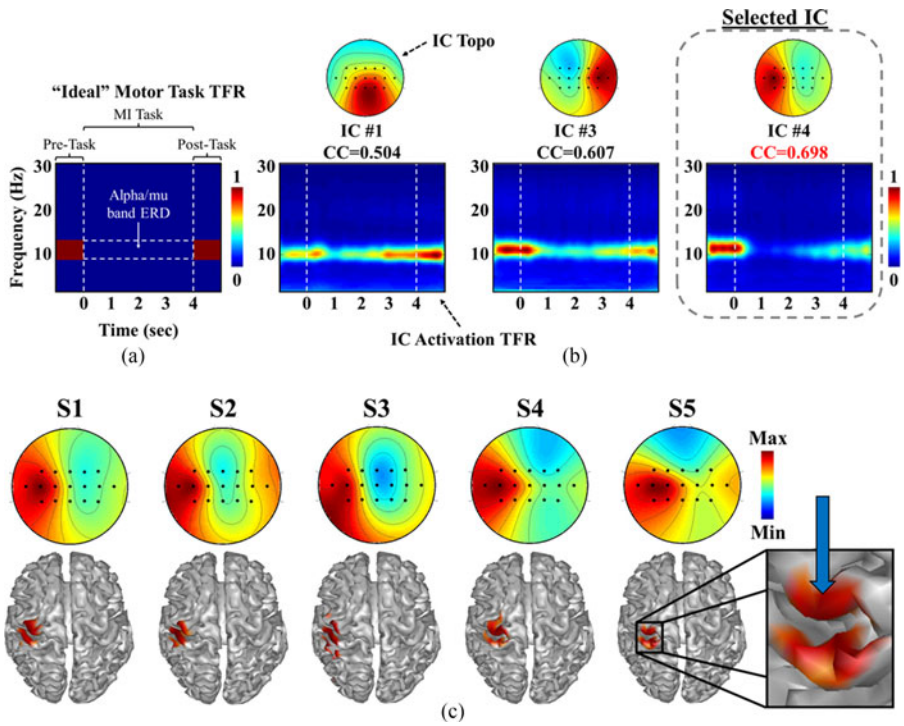

Fig. 3. (a) Ideal time–frequency response of motor task activity based on known neurophysiologic principles. A strong idling synchrony occurs in the alpha/mu band prior to the task (before 0 s). An alpha/mu desynchronization (ERD) occurs while performing the motor task (0–4 s) and resynchronizes after the task (after 4 s). (b) IC topographies and TFRs of the IC activation time series for the three ICs with a correlation coefficient (CC) above 0.50 with the idealized task for a representative subject. In this case, the right most IC (#4) was selected as the IC containing the motor information. (c) Selected IC topography and corresponding cortical ROI for each of the five subjects. For each subject, the selected IC topography was mapped onto a template brain using the WMNE and thresholded at 75% of the peak value to find the ROI boundaries. The blue arrow on the right highlights the hand knob of the precentral gyrus that is contained in all ROIs.

half-maximum (FWHM) of its Gaussian kernel, as seen in (4). The central frequency was chosen as 1 Hz, and the FWHM of the Gaussian kernel at the central frequency, FWHM_{f_c}, was chosen as 3 s [42]. The wavelet's length was then scaled for all other frequencies f by means of (5) to better capture the varying components of oscillatory activity. The wavelet coefficients were then calculated via (6) at 0.5-Hz intervals and convolved with the selected waveforms.

$$\sigma_{t,f_c} = \frac{\mathrm{FWHM}_{f_c}}{\sqrt{8\ln(2)}} \tag{4}$$

$$\sigma_{t,f} = \frac{\sigma_{t,f_c} f_c}{f} \tag{5}$$

$$\psi_f = \left(\sigma_{t,f}\sqrt{\pi}\right)^{-\frac{1}{2}} \cdot e^{\frac{t^2}{2\sigma_{t,f}^2}} \cdot e^{2\pi i f_c t} \tag{6}$$

Time–frequency features were extracted by breaking the TFRs into time windows and frequency bands that maximized classification accuracy. The most discriminable features were found using the Mahalanobis distance (MD), (7), a statistical measure of similarity between two distributions, X_1 and X_2, based on their respective means, μ_1 and μ_2, and the pooled covariance, Σ:

$$d^2 = (\mu_1 - \mu_2)\sum^{-1}(\mu_1 - \mu_2)^T \tag{7}$$

Finding individual features that yield the largest MDs is not optimal because when combined together to train a classifier, destructive interference may decrease the discriminability of the shared feature space. Therefore, we elected to use an iterative search method to find the top features which synergistically maximize the MD for any number of selected features [38], [43]. This approach found each successive feature by considering all remaining individual features and determined that which maximized the MD to be the next best feature. This practice ranks features for each task in multivariate space and ensures that the optimal combination of features is selected for classification analysis.

The MD, however, is best suited for binary applications, and therefore, in order to find those features that would best separate the four MI tasks examined in this study, a one-versus-rest approach was applied to each task. In these cases, X_1 represents the feature space from one of the four tasks, and X_2 the compiled feature space from the three other tasks. Hence, the features identified using the one-versus-rest approaches are those that were most unique to any one of the MI tasks. The most discriminable features from each task were concatenated and extracted from all tasks for the four-class classification to ensure that the same features were being compared.

A fivefold cross-validation procedure was implemented using 80% training and 20% testing sets. For each of the five folds, new features were extracted from each of the four tasks in the

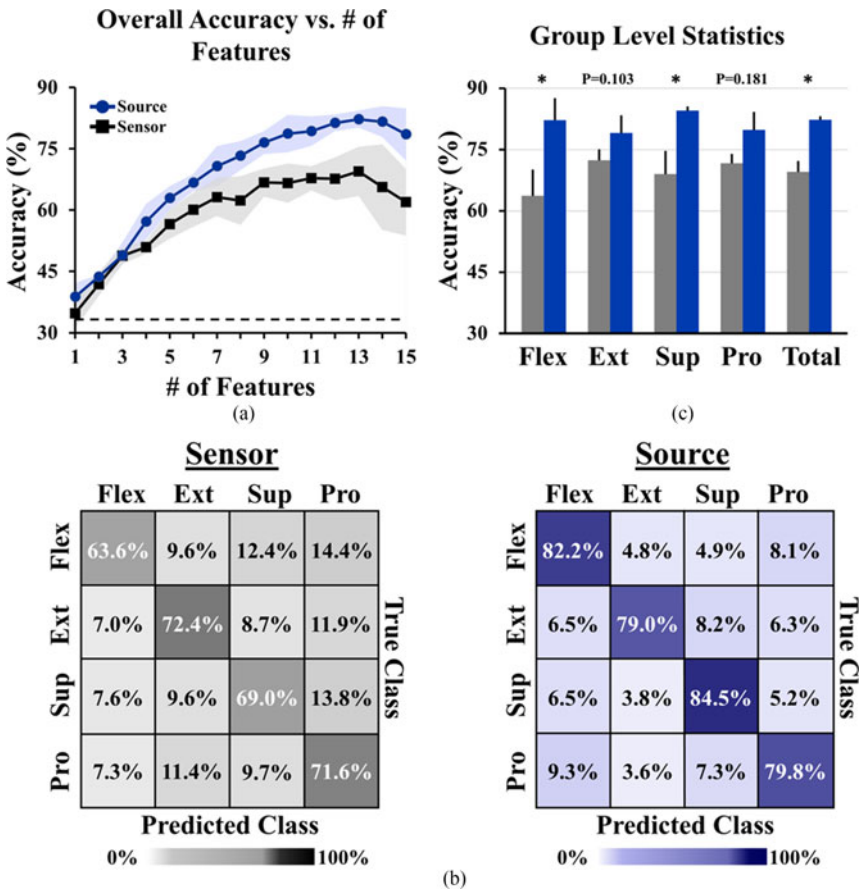

Fig. 4. (a) Overall classification rate of the four MI tasks using the sensor- and source-based methods plotted as a function of the number of top features used. The maximum accuracy for both methods was achieved when using 13 of the top features. (b) Confusion matrices for the sensor- and source-based methods at their respective peak overall accuracy (Flex—flexion, Ext—extension, sup—Supination, Pro—pronation). (c) Paired t-test results comparing the two methods on the individual task and overall basis at the peak overall accuracy of each domain ($^*p < 0.05$). Bar graphs are shown with standard error.

training set and applied to the corresponding testing set for classification.

F. Classification

A MD-based classifier was used for the four-class classification analysis [40]. The classifier was constructed by finding the mean, μ_i, and covariance, $\sum_i$, of the training samples from each of the four tasks ($i = 4$). For any testing sample y, the MD was found between each of the four class distributions and was ultimately assigned to the class which minimized the distance, as described by:

$$\min_i \sqrt{(y-\mu_i)\sum_i{}^{-1}(y-\mu_i)^T} \tag{8}$$

For the testing samples belonging to a particular task, the classifier's output was compared with the true class in a standard confusion matrix. Classification accuracy for each task was computed by dividing the number of correctly identified samples by the total number of testing samples belonging to the same class. Thus, the classification percentages sum to 100% along each row of the confusion matrix. To obtain an overall classification measure, the sum of the values along the diagonal of the confusion matrix was divided by the total number of samples in the entire testing set. The same analysis was performed on all sensor waveforms and compared with the proposed source imaging method.

III. Results

A. Classification Accuracy

The group-averaged overall classification accuracy is displayed in Fig. 4(a) as a function of the feature space dimension. Using few features, classification in the two domains is nearly identical; however, as the number of features increases, there emerges a clear separation between the sensor space and source space accuracy, peaking at 69.5% and 82.2%, respectively. Both domains achieved their maximum overall accuracy when using 13 of the most discriminable features. An adjusted Wald's test was used to calculate a confidence interval of 25.8±7.5% for chance performance of the classifier [44], the upper bound of which is plotted in Fig. 4(a) alongside the classification rates. The confusion matrices in Fig. 4(b) illuminate the group-level classification results for the four tasks at each domain's respective maximum accuracy. On the individual task basis, the source space classification outperformed that of sensor space for all four tasks with an improvement rate between 6.6% and 18.6%.

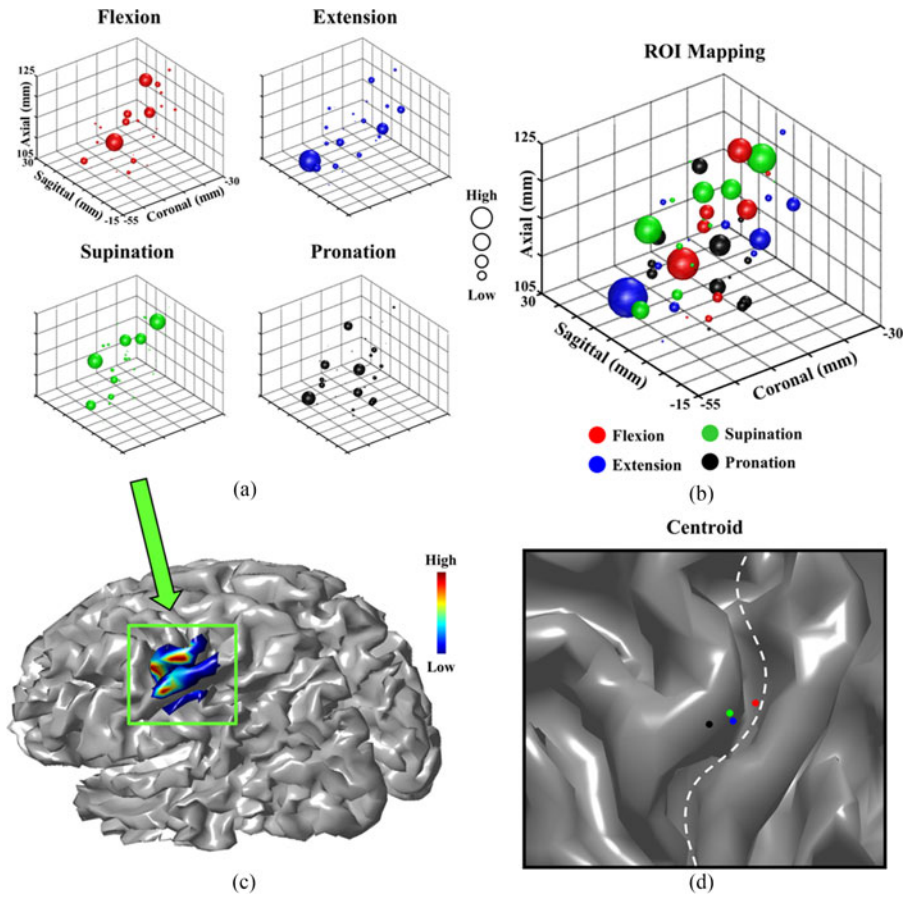

Fig. 5. (a) Spatial distribution of the top features for each task within the ROI in a representative subject. The size of the sphere indicates the contribution of that dipole location for separating a given task from the other three, with the largest sphere indicating the strongest representation. (b) To map the ROI, each dipole within the ROI was assigned to the task which had the largest representation in the source space. (c) Spatial distribution of supination was projected onto a rendered brain to visualize the spatial distribution on the cortex. Warm colors signify the larger sphere sizes depicted in (a), whereas cool colors signify smaller spheres. (d) Centroids of each MI task's distribution localized on or near the hand knob of the precentral gyrus. The white dotted line indicates the central sulcus.

Fig. 4(c) displays the group-level statistical results of each of the four MI tasks at the maximum overall accuracy achieved in the sensor and source domains. The sensor domain outperformed the source domain in only three subject-imagination pairings; pronation in S1 and S4, and extension in S2. The overall peak accuracies in the sensor and source domains are shown on the far right of Fig. 4(c). A paired t-test was used to determine the statistical significance between the source- and sensor-based methods on the task accuracies and overall accuracy. As indicated by Fig. 4(c), the source method proved to significantly ($p < 0.05$) improve the accuracy of flexion ($p = 0.007$), supination ($p = 0.038$), and the total accuracy ($p = 0.006$). We also tested the classification results against chance using a bootstrap method by selecting random samples ($n = 5$) within the aforementioned confidence interval. The results of a paired t-test revealed that all of the task accuracies and the overall accuracy in both domains were significantly different from chance ($p < 0.05$).

B. Cortical Mapping

For all five subjects, there clearly emerged a single component with the highest correlation with the motor task; the subsequent ROIs localized to the left sensorimotor cortex and encompass the hand knob of the precentral gyrus. The features that maximized the overall classification were traced back to their location in the corresponding spatial, temporal, and spectral domains to observe signals responsible for separating each task.

Each one of the selected features corresponds to a particular time window and frequency band of a single dipole's time series within the right-hand cortical ROI. The ranking procedure used in selecting the time–frequency features utilizes the MD as an indicator of separation between each one-versus-rest comparison (one task versus the other three). Therefore, not all features will contribute equally; the increase of the MD upon adding a new feature can be used to measure the influence of that feature on separating the task in question from the other three. When tracing features to their respective domain, each feature was weighted by the percent increase of the MD that resulted when that particular feature was added.

In the spatial domain, some dipoles may contain more than one of the top features, while others may contain none of the top features. Spatial source-based feature maps for each of the four MI tasks in a representative subject are displayed in Fig. 5(a). The increasing size of the sphere indicates the higher

TABLE I
PAIRWISE R^2 VALUES OF THE CORTICAL ROI SPATIAL FEATURE MAPS BETWEEN ALL COMBINATIONS OF THE FOUR MI TASKS

Subject	F–E	F–S	F–P	E–S	E–P	S–P
1	0.007	0.027	0.010	0.005	0.009	0.031
2	0.118	0.001	0.026	0.133	0.001	0.056
3	0.014	0.015	0.011	0.027	#	0.044
4	#	0.266	0.167	0.046	0.005	0.096
5	0.015	0.043	0.007	0.041	0.006	0.016
Average	**0.031**	**0.071**	**0.044**	**0.050**	**0.004**	**0.049**

# denotes values less than 0.001. F—flexion, E—Extension, S—Supination, P—Pronation

contribution of that particular dipole to the unique characteristics of the indicated task. We noticed that some dipoles were very important (large sphere) for multiple tasks and, therefore, attempted to map the ROI by finding, for each dipole, the best represented MI task. In this sense, each dipole was assigned to a single task with the strongest representation in the communal space, as seen in Fig. 5(b). In Fig. 5(c), one of the four tasks was superimposed on a rendered brain to highlight the distribution in terms of an anatomical model.

To determine the spatial relationships between the four tasks' cortical representations, we computed pairwise spatial correlations for all combinations of the four tasks. The R^2 values for all subjects are displayed in Table I. No consistent correlation patterns emerged across subjects, indicating that the spatial distributions were quite distinct for each task.

Features were also traced back in the spectral and temporal domains such that the different frequency bands and time windows containing the most discriminable information could be identified. For each task, the spectral-temporal feature maps can be represented as time–frequency distributions where the darker time–frequency block indicates the higher contribution to separating each task from the others (similar to the size of the sphere in the spatial domain). Fig. 6 displays the group averaged time–frequency feature maps for each of the four MI tasks. Histograms below and to the right of each TFR provide a summary of the feature distribution in the respective domain. Features can be seen to be distributed throughout the trials with various peaks in the delta, alpha/mu, and beta bands.

IV. DISCUSSION

The integration of noninvasive BCIs into everyday use is pushing the limit of our ability to interpret a user's motor intent solely through signals detected at the scalp [1], [11], [12]. SMR BCIs in particular have been incorporated into many real-life situations by controlling devices such as wheelchairs [45], limb orthoses [46], or quadcopters [16]. The success of these systems is in large part due to the ability to exploit the underlying neurophysiological processes of the primary sensorimotor cortex. The spatial location and time-varying behavior of rhythmic components of EEG signals can often dissociate different activation patterns originating on the cortical surface; however, the low spatial resolution of EEG limits the number of patterns that can be separated. Therefore, SMR BCIs that are in fact able to achieve successful higher dimensional control often utilize MI tasks that are not associated with the output action that the user is attempting to complete, and rather are used simply because the tasks are easily separated. This study aimed to address this concern by using ESI techniques to investigate the separability of four MI tasks involving complex manipulations of the right hand: flexion, extension, supination, and pronation. The results indicate that ESI is able to greatly improve the classification of these four tasks over traditional sensor techniques.

The basic principle of EEG inverse transforms are to project the electrical values recorded on the scalp over a discrete geometrical representation of the brain [19], [47]. In this sense, the information collected by the EEG can be constrained to include information from anatomical structures that are more correlated with the task being performed [22]–[28]. In order to constrain the cortical activity, an ROI was derived from a single component of the compiled MI task data. The component was selected purely based on the highest time–frequency correlation with an ideal MI task; for all subjects, the selected component also displayed the following:

1) focal activity overlying the left (contralateral) motor cortex;
2) spectral-temporal behavior displaying ERD in the alpha/mu band at the onset of the task.

Our data-driven approach of identifying cortical ROIs containing distinct task information was consistent with previous source localization results of finding brain regions responsible for right-hand MI tasks [22], [48]. In finding these ROIs using the compiled data from all four MI tasks, the selected ROI was derived from the overlapping source activity of the right hand rather than any single task. By doing so, bias toward any one of the four MI tasks should, therefore, cancel out such that information from each task is equally represented within the ROI. We can see from the mapping in Fig. 5(b) that no one task dominates the ROI and that all tasks are well embodied within the right-hand space. The centroids of the spatial networks also localize to similar sites on or near the precentral gyrus [see Fig. 5(d)] for all five subjects. These two observations indicate that none of the tasks were underrepresented or had a spatial preference, but rather that the data-driven ROI identification evenly captured discriminable information from each task.

The classification of the four tasks displayed a global increase of 12.7% in the source domain compared to the sensor domain [see Fig. 4(a)]. This enhancement is nearly double that (7.1%) which was found in our previous work on separating left- and right-hand MI tasks using source analysis [26]. However, the previous study involved only a binary classification, whereas in this study, four tasks are being separated [26]; with the increased number of tasks, this improvement is even more substantial.

Among the tasks in question, flexion saw the greatest single task improvement (18.6%), while the smallest improvement was seen in extension (6.6%). We believe this phenomenon partially stems from the user's ability to perform the different MI tasks; when asked about the difficulty in performing each task, subjects often reported that flexion felt the most natural and was the

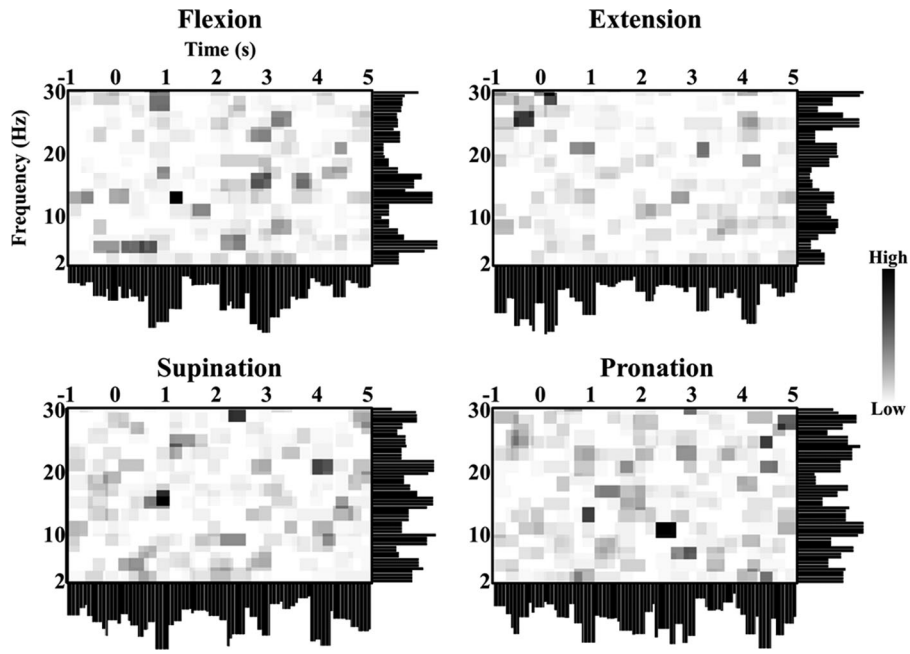

Fig. 6. Group averaged feature mapping in the time and frequency domains. Histograms below and to the right of the time–frequency plots sum the features in each domain to show the importance of each time window and frequency band for discriminating each task from the other three. The darker the blocks in the plots indicate higher importance for the specified task.

easiest to visualize mentally. On the other hand, either supination or extension was reported to be the most unnatural MI task to perform.

Furthermore, the results were not biased by pairing flexion and extension, and supination and pronation MI tasks together within a single run. Transient nonstationarities in the EEG are likely to cluster within a single run, rather than be spread across multiple runs or days. The resulting prejudice would likely cause the most common misclassifications to be between the tasks within each pairing; however, we did not observe any such trend. Rather, we observed higher misclassification rates between tasks that were most similar in terms of the physical action; flexion (bend inward) and pronation (twist inward), and extension (bend outward) and supination (twist outward). We also noticed that this phenomenon occurred primarily in the source domain. For example, in the source confusion matrix in Fig. 4(b), the flexion task's most prevalent false negative was pronation, as was supination for the extension task and flexion for the pronation task. In the sensor confusion matrix, this effect is only observed by flexion most commonly misclassified as pronation. This trend supports the idea that even though subjects were not actually executing the motion, the signals generated from imagining the movement were still representative of the different tasks. Furthermore, the higher spatial resolution achieved through ESI techniques may help to illuminate the subtle differences in these signals [49].

Penfield's classical definition of somatotopy within the primary motor cortex dedicated independent cortical regions to the control of single muscles or body parts. However, it has since been observed in humans using electrocorticography [50], [51] and functional MRI [52]–[54] recordings that there is clear overlap in the activation of neural circuits both during tasks of different limbs and of the same limb, most notably the hand. The cause of this overlap is thought to stem from horizontal connections within the hand region of the cortex where different populations of cells are responsible for moving some parts of the hand while withholding the movement of others [55]. The result is a distributed activation pattern that dynamically changes based on the type of action being performed and the involvement of the different muscles and joints. These results have led to the development of a modern theory of hierarchical encoding of M1 where individual cells encode for combined muscle movements, with a map of functional tasks overlaid on top of the dynamic topographical boundaries [56], [57].

In tracing features responsible for separating each task to their respective cortical locations [see Fig. 5(a)], we were able to observe overlapping and yet distinct distributed networks among the dipoles in the right-hand ROI that support a functional somatotopic representation of M1. The results from Table I describing the spatial correlations between the different tasks display no consistent similarities across tasks or subjects and suggest unique task-based interactions between the different dipoles in the ROI. Nevertheless, the current density reconstruction resulting from ESI techniques is not a true restoration of neuronal behavior, but rather an estimation of the current density at discrete points in brain space. However, by increasing the sampling density of the data and incorporating additional anatomical information through ESI, we were able to emulate dipole interactions that may be more similar to the underlying neurophysiology than can be achieved in the sensor domain. By doing so, representative activity of smaller neuronal populations (compared to sensor analysis) within the right-hand ROI was able to increase the separability of different MI tasks originating in the same region.

When examining the features in the time domain (see Fig. 6), there appeared to be a fairly even distribution across the entire trial. This indicates that discriminable information can be detected from continuously performing the tasks rather than at a specific time point/windows relative to the task onset. When examining the frequency histograms, we found that there were often peaks in the delta and alpha/mu bands and multiple peaks in the beta band. A wide range of frequency bands have been attributed to distinct traces of motor intention. Studies by Vučković and Sepulveda [58], [59] examined MI tasks similar to the present study and found that the delta band carried the most class-specific information. Activity in the alpha/mu, beta, and gamma (>35 Hz) bands has also been shown to carry discriminable information relevant to these types of tasks [59]–[62]. Pairwise binary classification schemes are often used in these studies to achieve accuracies as high as >80% making results difficult to compare to the present study; however, the current work achieved similar accuracies (82.2%) using twice as many classes demonstrating much increased performance with the proposed ESI approach.

The current results were based on using the combination of information from multiple-frequency bands and we cannot draw concrete conclusions as to which frequency band contributed most to the discrimination of the four tasks. Further analysis using information from each frequency band independently [63]–[65] would be needed to determine which frequencies contain the most discriminable information regarding these tasks.

In all, the defining spatial, temporal, and spectral characteristics of the MI tasks exposed in this study are consistent with documented neurophysiological evidence using other neuroimaging modalities. The overlapping band-specific oscillatory activity in the shared cortical region allowed us to successfully separate MI tasks involving complex manipulations of the right hand.

V. Conclusion

Introduction of complex MI tasks of the same limb into SMR BCIs can drive these systems toward user-centered applications in which specific jobs can be integrated depending on the user's personal needs. It is unrealistic to construct a noninvasive SMR BCI to accomplish tasks involving all the degrees of freedom of the human hand; however, in reality, users of these systems will need only a limited number of tasks to increase their autonomy. These tasks will need to be easy for the users to perform, and as such, an intuitive connection between the MI tasks used to accomplish an action is imperative. The present study aimed to determine if complex tasks of the hand could be separated for this exact purpose. Most everyday tasks such as picking up a cup or turning ON and OFF a light switch involve fine motor control of the hand; therefore, we investigated MI tasks that imitated complex manipulations of the hand that may be of use for accomplishing these tasks.

In conclusion, this study for the first time reports the application of ESI techniques to separating multiple MI tasks of the same hand. The results indicate that MI tasks involving different orientations of the right hand can be classified with high accuracy and can be enhanced through ESI techniques. The successful integration of these tasks into a source-analysis-based BCI may help subjects for the self-modulation of brain states associated with actions that can be useful on a day-to-day basis.

Acknowledgment

The authors are grateful to C. Zhang and L. Yu for helpful discussions and to T. Hanson for aiding in data collection.

References

[1] B. He *et al.*, "Brain-computer interface," in *Neural Engineering*, 2nd ed., B. He, Ed. Boston, MA, USA: Springer, 2013, pp. 87–151.
[2] J. L. Collinger *et al.*, "High-performance neuroprosthetic control by an individual with tetraplegia," *Lancet*, vol. 381, pp. 557–564, Feb. 2013.
[3] L. R. Hochberg *et al.*, "Reach and grasp by people with tetraplegia using a neurally controlled robotic arm," *Nature*, vol. 485, pp. 372–375, May 2012.
[4] E. Donchin *et al.*, "The mental prosthesis: Assessing the speed of a P300-based brain-computer interface," *IEEE Trans. Rehabil. Eng.*, vol. 8, no. 2, pp. 174–179, Jun. 2000.
[5] C.-C. Postelnicu and D. Talaba, "P300-based brain-neuronal computer interaction for spelling applications," *IEEE Trans. Biomed. Eng.*, vol. 60, no. 2, pp. 534–543, Feb. 2013.
[6] Y. Li *et al.*, "A hybrid BCI system combining P300 and SSVEP and its application to wheelchair control," *IEEE Trans. Biomed. Eng.*, vol. 60, no. 11, pp. 3156–3166, Nov. 2013.
[7] Y. Kimura *et al.*, "SSVEP-based brain-computer interfaces using FSK-modulated visual stimuli," *IEEE Trans. Biomed. Eng.*, vol. 60, no. 10, pp. 2831–2838, Oct. 2013.
[8] S. Gao *et al.*, "Visual and auditory brain-computer interfaces," *IEEE Trans. Biomed. Eng.*, vol. 61, no. 5, pp. 1436–1447, May 2014.
[9] E. Yin *et al.*, "A speedy hybrid BCI spelling approach combining P300 and SSVEP," *IEEE Trans. Biomed. Eng.*, vol. 61, no. 2, pp. 473–483, Feb. 2014.
[10] R. Xu *et al.*, "Enhanced low-latency detection of motor intention from EEG for closed-loop brain-computer interface applications.," *IEEE Trans. Biomed. Eng.*, vol. 61, no. 2, pp. 288–296, Feb. 2014.
[11] H. Yuan and B. He, "Brain-computer interfaces using sensorimotor rhythms: Current state and future perspectives," *IEEE Trans. Biomed. Eng.*, vol. 61, no. 5, pp. 1425–1435, May 2014.
[12] B. He *et al.*, "Noninvasive brain-computer interfaces based on sensorimotor rhythms," *Proc. IEEE*, vol. 103, no. 6, pp. 907–295, Jun. 2015.
[13] J. R. Wolpaw and D. J. McFarland, "Control of a two-dimensional movement signal by a noninvasive brain-computer interface in humans," *Proc. Nat. Acad. Sci. U.S.A.*, vol. 101, no. 51, pp. 17849–17854, Dec. 2004.
[14] A. Royer *et al.*, "EEG control of a virtual helicopter in 3-dimensional space using intelligent control strategies," *IEEE Trans. Neural Syst. Rehabil. Eng.*, vol. 18, no. 6, pp. 581–589, Dec. 2010.
[15] A. J. Doud *et al.*, "Continuous three-dimensional control of a virtual helicopter using a motor imagery based brain-computer interface," *PLoS One*, vol. 6, no. 10, p. e26322, Jan. 2011.
[16] K. LaFleur *et al.*, "Quadcopter control in three-dimensional space using a noninvasive motor imagery-based brain-computer interface," *J. Neural Eng.*, vol. 10, no. 4, p. 046003, Aug. 2013.
[17] G. Pfurtscheller and L. D. Silva, "Event-related EEG/MEG synchronization and desynchronization: Basic principles," *Clin. Neurophysiol.*, vol. 110, no. 11, pp. 1842–1857, 1999.
[18] K. Cassady *et al.*, "The impact of mind-body awareness training on the early learning of a brain-computer interface," *Technology*, vol. 2, no. 3, pp. 254–260, Mar. 2014.
[19] B. He and L. Ding, "Electrophysiological neuroimaging," in *Neural Engineering*, 2nd ed., B. He, Ed. Boston, MA, USA: Springer, 2013, pp. 499–543.
[20] D. Wang *et al.*, "Multi-class motor imagery EEG decoding for brain-computer interfaces," *Front. Neurosci.*, vol. 6, p. 151, Jan. 2012.
[21] A. Schlögl *et al.*, "Characterization of four-class motor imagery EEG data for the BCI-competition 2005," *J. Neural Eng.*, vol. 2, no. 4, pp. L14–L22, Dec. 2005.
[22] H. Yuan *et al.*, "Cortical imaging of event-related (de) synchronization during online control of brain-computer interface using minimum-norm

estimates in frequency domain," *IEEE Trans. Neural Syst. Rehabil. Eng.*, vol. 16, no. 5, pp. 425–431, Oct. 2008.
[23] H. Yuan *et al.*, "Negative covariation between task-related responses in alpha/beta-band activity and BOLD in human sensorimotor cortex: An EEG and fMRI study of motor imagery and movements," *Neuroimage*, vol. 49, no. 3, pp. 2596–2606, Feb. 2010.
[24] L. Qin *et al.*, "Motor imagery classification by means of source analysis for brain-computer interface applications," *J. Neural Eng.*, vol. 1, no. 3, pp. 135–141, Sep. 2004.
[25] B. Kamousi *et al.*, "Classification of motor imagery tasks for brain-computer interface applications by means of two equivalent dipoles analysis," *IEEE Trans. Neural Syst. Rehabil. Eng.*, vol. 13, no. 2, pp. 166–171, Jun. 2005.
[26] B. Kamousi *et al.*, "Classification of motor imagery by means of cortical current density estimation and Von Neumann entropy," *J. Neural Eng.*, vol. 4, no. 2, pp. 17–25, Jun. 2007.
[27] M. Mattiocco *et al.*, "Neuroelectrical source imaging of mu rhythm control for BCI applications," in *Proc. 28th Annu. Int. IEEE EMBS Conf.*, 2006, vol. 1, pp. 980–983.
[28] F. Cincotti *et al.*, "High-resolution EEG techniques for brain-computer interface applications," *J. Neurosci. Methods*, vol. 167, no. 1, pp. 31–42, Jan. 2008.
[29] A. N. Tikhonov and V. Y. Arsenin, "Solutions of ill-posed problems," *Am. Math. Soc.*, vol. 32, no. 144, pp. 1320–1322, 1977.
[30] R. D. Pascual-Marqui *et al.*, "Low resolution electromagnetic tomography: A new method for localizing electrical activity in the brain," *Int. J. Psychophysiol.*, vol. 18, no. 1, pp. 49–65, Oct. 1994.
[31] C. J. Holmes *et al.*, "Enhancement of MR images using registration for signal averaging," *J. Comput. Assist. Tomogr.*, vol. 22, no. 2, pp. 324–333, 1998.
[32] B. He *et al.*, "Electric dipole tracing in the brain by means of the boundary element method and its accuracy," *IEEE Trans. Biomed. Eng.*, vol. BME-34, no. 6, pp. 406–414, Jun. 1987.
[33] M. S. Hämäläinen and J. Sarvas, "Realistic conductivity geometry model of the human head for interpretation of neuromagnetic data," *IEEE Trans. Biomed. Eng.*, vol. 36, no. 2, pp. 165–171, Feb. 1989.
[34] T. F. Oostendorp *et al.*, "The conductivity of the human skull: Results of in vivo and in vitro measurements," *IEEE Trans. Biomed. Eng.*, vol. 47, no. 11, pp. 1487–1492, Nov. 2000.
[35] Y. Zhang *et al.*, "Estimation of in vivo brain-to-skull conductivity ratio in humans," *Appl. Phys. Lett.*, vol. 89, p. 223903, 2006.
[36] Y. Lai *et al.*, "Estimation of in vivo human brain-to-skull conductivity ratio from simultaneous extra- and intra-cranial electrical potential recordings," *Clin. Neurophysiol.*, vol. 116, pp. 456–465, 2005.
[37] D. Mattia *et al.*, "Motor-related cortical dynamics to intact movements in tetraplegics as revealed by high-resolution EEG," *Hum. Brain Mapp.*, vol. 27, no. 6, pp. 510–519, Jun. 2006.
[38] B. Edelman *et al.*, "Decoding and mapping of right hand motor imagery tasks using EEG source imaging," in *Proc. 7th Annu. Int. IEEE EMBS Neural Eng. Conf.*, 2015, pp. 194–197.
[39] J. Cardoso, "Infomax and maximum likelihood for blind source separation," *IEEE Signal Process. Lett.*, vol. 4, no. 4, pp. 112–114, Apr. 1997.
[40] G. Pfurtscheller *et al.*, "Mu rhythm (de)synchronization and EEG single-trial classification of different motor imagery tasks," *Neuroimage*, vol. 31, no. 1, pp. 153–159, May 2006.
[41] G. Pfurtscheller *et al.*, "EEG-based discrimination between imagination of right and left hand movement," *Electroencephalogr. Clin. Neurophysiol.*, vol. 103, no. 6, pp. 642–651, Dec. 1997.
[42] F. Tadel *et al.*, "Brainstorm: A user-friendly application for MEG/EEG analysis," *Comput. Intell. Neurosci.*, vol. 2011, p. 879716, Jan. 2011.
[43] B. Edelman *et al.*, "Discriminating hand gesture motor imagery tasks using cortical current density estimation," in *Proc. 37th Annu. Int. IEEE EMBS Conf.*, 2014, pp. 1314–1317.
[44] G. R. Müller-Putz *et al.*, "Better than random? A closer look on BCI results," *Int. J. Bioelectromagn.*, vol. 10, no. 1, pp. 52–55, 2008.
[45] R. Leeb *et al.*, "Self-paced (asynchronous) BCI control of a wheelchair in virtual environments: A case study with a tetraplegic," *Comput. Intell. Neurosci.*, vol. 2007, p. 79642, Jan. 2007.
[46] G. Pfurtscheller *et al.*, "Brain oscillations control hand orthosis in a tetraplegic," *Neurosci. Lett.*, vol. 292, no. 3, pp. 211–214, Oct. 2000.
[47] B. He *et al.*, "Electrophysiological imaging of brain activity and connectivity-challenges and opportunities," *IEEE Trans. Biomed. Eng.*, vol. 58, no. 7, pp. 1918–1931, Jul. 2011.
[48] W. Wang *et al.*, "Decoding and cortical source localization for intended movement direction with MEG," *J. Neurophysiol.*, vol. 104, no. 5, pp. 2451–2461, Nov. 2010.
[49] B. He *et al.*, "Grand challenges in mapping the human brain: NSF workshop report," *IEEE Trans. Biomed. Eng.*, vol. 60, no. 11, pp. 2983–2992, Nov. 2013.
[50] J. Kubánek *et al.*, "Decoding flexion of individual fingers using electrocorticographic signals in humans," *J. Neural Eng.*, vol. 6, no. 6, p. 066001, Dec. 2009.
[51] T. Pistohl *et al.*, "Decoding natural grasp types from human ECoG," *Neuroimage*, vol. 59, no. 1, pp. 248–260, Jan. 2012.
[52] J. Sanes *et al.*, "Shared neural substrates controlling hand movements in human motor cortex," *Science*, vol. 268, no. 5218, pp. 1775–1777, 1995.
[53] J. D. Meier *et al.*, "Complex organization of human primary motor cortex: A high-resolution fMRI study," *J. Neurophysiol.*, vol. 100, no. 4, pp. 1800–1812, Oct. 2008.
[54] P. Hlustík *et al.*, "Somatotopy in human primary motor and somatosensory hand representations revisited," *Cereb. Cortex*, vol. 11, no. 4, pp. 312–321, Apr. 2001.
[55] M. H. Schieber and L. S. Hibbard, "How somatotopic is the motor cortex hand area?," *Science*, vol. 261, no. 5120, pp. 489–492, 1993.
[56] M. Flanders, "Functional somatotopy in sensorimotor cortex," *Neuroreport*, vol. 16, no. 4, pp. 313–316, Mar. 2005.
[57] R. N. Holdefer and L. E. Miller, "Primary motor cortical neurons encode functional muscle synergies," *Exp. Brain Res.*, vol. 146, no. 2, pp. 233–243, Sep. 2002.
[58] A. Vučković and F. Sepulveda, "Delta band contribution in cue based single trial classification of real and imaginary wrist movements," *Med. Biol. Eng. Comput.*, vol. 46, no. 6, pp. 529–539, Jun. 2008.
[59] A. Vučković and F. Sepulveda, "A two-stage four-class BCI based on imaginary movements of the left and the right wrist," *Med. Eng. Phys.*, vol. 34, no. 7, pp. 964–971, Sep. 2012.
[60] E. López-Larraz *et al.*, "Continuous decoding of movement intention of upper limb self-initiated analytic movements from pre-movement EEG correlates," *J. Neuroeng. Rehabil.*, vol. 11, p. 153, Jan. 2014.
[61] Y. Gu *et al.*, "Single-trial discrimination of type and speed of wrist movements from EEG recordings," *Clin. Neurophysiol.*, vol. 120, no. 8, pp. 1596–600, Aug. 2009.
[62] Y. U. Khan and F. Sepulveda, "Brain–computer interface for single-trial EEG classification for wrist movement imagery using spatial filtering in the gamma band," *IET Signal Process.*, vol. 4, no. 5, pp. 510–517, 2010.
[63] S. Waldert *et al.*, "Hand movement direction decoded from MEG and EEG," *J. Neurosci.*, vol. 28, no. 4, pp. 1000–1008, 2008.
[64] T. J. Bradberry *et al.*, "Reconstructing three-dimensional hand movements from noninvasive electroencephalographic signals," *J. Neurosci.*, vol. 30, no. 9, pp. 3432–3437, Mar. 2010.
[65] T. M. Hall *et al.*, "A common structure underlies low-frequency cortical dynamics in movement, sleep, and sedation," *Neuron*, vol. 83, no. 5, pp. 1185–1199, Sep. 2014.

Authors' photographs and bioraphies not available at the time of publication.